A novel morphing propeller system inspired by origami-based structure

Kan Ye [1]

School of Mechanical and Mechatronic Engineering

University of Technology Sydney, 15 Broadway, Ultimo, NSW 2007, Australia

kan.ye@uts.edu.au

J.C. Ji

School of Mechanical and Mechatronic Engineering

University of Technology Sydney, 15 Broadway, Ultimo, NSW 2007, Australia

jin.ji@uts.edu.au

ABSTRACT

For a standard propeller system, the thrust output and the energy dissipation are proportionally dependent on its rotating speed, as its physic characteristics and working conditions are normally fixed during its operation. In order to improve the system performance and meet special application requirements, this paper presents the design of a novel two-stage propeller system with morphing blade structure for higher thrust output and energy efficiency in operations. Based on the stacked Miura-ori (SMO) pattern, an origami-based structure is designed to enable a change in blade length for a propeller system and thus to improve the system performance. The unique snap-through feature of the proposed origami structure is

[1] Corresponding author

utilized to provide a two-stage working condition according to its rotating speed. The geometric parameter analysis of the SMO structure is first investigated, specifically focusing on the operating mechanism due to the snap-through behavior. Then the implementation of the SMO structure into a rotating system is studied. The effects of design parameters on the critical transition points, which correspond to two operating states of the proposed propeller system, are numerically discussed. The simulation results confirm the performance improvement on the thrust output and energy saving. The feasibility of using origami-based structure provides valuable insights into more applications in similar domains, such as fan system and wind turbine blades.

1 INTRODUCTION

For a standard propeller system, its physical parameters such as blade shape, pitch angle and effective blade length, and the working condition such as fluid density, are normally fixed once the propeller system is deployed in service. According to those characteristics, the only method of controlling the thrust output and the energy dissipation is by changing the rotating speed. In order to provide an alternative control method, morphing structures have been applied in designing aircraft wings [1] and wind turbine blades [2]. By changing the shape of the structures, the geometric property and the system performance can be switched into different states. Control approaches of the morphing wings and blades were discussed as active-tip [3] or active flap [4]. With these morphing structure, the torsional loads at the blade root and vibrations on the structure could be reduced. Other morphing technologies without the aerofoil change of the wings or blades include span-wise using telescopic structure and active twist. In such cases, the complex aerodynamic problem due to the aerofoil change could be avoided. Blondeau et al. [5] developed a telescopic wing to increase the aerodynamic loads. The extendable

wings were configured by using inflatable spars and concentric aluminum tubes. Dam et al. [6] investigated a span-wise morphing blade. An extending tip blade was used to increase the blade length when required.

Origami-based structures, as a specific form of the morphing structures, have shown their advantages over other types of morphing structures [7], including compact deployment, storage capability and re-configurability. Origami structures can be stored in a small size when folded and be used in a full size when deployed. Based on these features, various origami structures for static application were developed, such as collapsible kayaks [8], oriceps [9] and medical devices [10-12]. The other features of origami structures, such as bistable state and self-deployable ability, were considered for dynamic applications [13-15]. In addition, the origami-based structures could be used for vibration isolation based on their nonlinear force-displacement relationships [16]. A typical origami pattern, the so called the stacked Miura-ori (SMO) pattern, is a double-layer structure with different Miura-ori cells stacked. This foldable metamaterial-like structure can produce an intrinsic bi-stability through its geometric configuration, where its unique kinematic constraint and snap-through behaviour would lead to asymmetric behaviour when it is switched between different stable states [17-19].

This paper presents the design of a novel two-stage origami-structure based morphing propeller system, in order to improve the system performance. The proposed morphing structure is realized by using the SMO structure to enable the self-change in blade length according to the rotating speed of the system, hence to change the effective propeller diameter. The SMO structure is incorporated into the rotating shaft system to

create a morphing blade system, enabling the morphing structure to quickly respond to the rotating speed and switch the blades between different lengths. Thus, improvement on the thrust output and energy saving can be achieved. The geometric parameter analysis on the SMO structure and the system performance are first investigated, specifically focusing on the operating mechanism from the unique snap-through behavior. Then system parameters of the SMO structure and the rotating system are numerically investigated to demonstrate their effects on the critical points. It is hoped that the proposed novel system can be applied and replace some existing structures with specific requirements on thrust output or energy saving.

The rest of this paper is organized into three sections. Section 2 presents the structural design of the proposed morphing system and its operating mechanism. Section 3 numerically studies the effects of the design parameters on the morphing performance. Concluding remarks are summarized in Section 4.

2 Design of the morphing propeller system

The proposed morphing propeller system includes two main components; the rotating system with extendable blade shell and the origami-based morphing structure, as shown in Fig. 1. A guide rod and mass weight are the linkage structures and shared by both components of the system.

The rotating system is composed of a rotating shaft and multiple extendable blades. The number of the blades should be an odd number to avoid the possible resonance when using an even-number blade system. Three blades are considered in this

paper and are designed with extendable shell components. The extension of the blade shell is synchronized with the deformation of the origami structure. In order to simplify the discussion of the blade's performance, regular propeller characteristics are used and the propeller coefficients for calculating its thrust output and the torque required are assumed to be constants. This means that the coefficients will not be changed if the blade length is changed, in order to simplify the comparison of the performance of the propeller system with two different blade lengths.

The morphing structure component uses the SMO structure to automatically adjust the effective length of the blade. The bottom end of the SMO structure is fixed on the guide rod and the other end of the SMO structure can perform free-sliding motion along the guide rod. A designed weight (mass block) is applied to the free-sliding end of the SMO structure and is jointed to the extendable blade shell. As such, the shape change of the SMO structure in the sliding direction would synchronize to the displacement of the weight and the extension of the blade shell. The centrifugal force of the designed weight due to the rotation of the system can be applied on the SMO structure and enable the SMO structure to switch between its two-stable states. Accordingly, the effective length of the blade, i.e., the effective propeller diameter, can be adaptively adjusted according to the rotational speed of the system. Fig. 1(c) and (d) illustrates the difference states of the SMO structure and the length change of a single blade. The two-stable states of the SMO structure are defined in Fig. 3(c). At the initial state (the rest state or non-operating condition), the SMO structure is at concave stable state and the length of the blade is kept minimum. At the working state, when the system rotates at different speeds,

the SMO structure can be switched between the concave state and convex state according to the centrifugal force and its asymmetric bi-stable states. Thus, this propeller system is equivalent to the mechanism of two propeller systems having two sets of different blade lengths, which is different from the standard system with the fixed length blades.

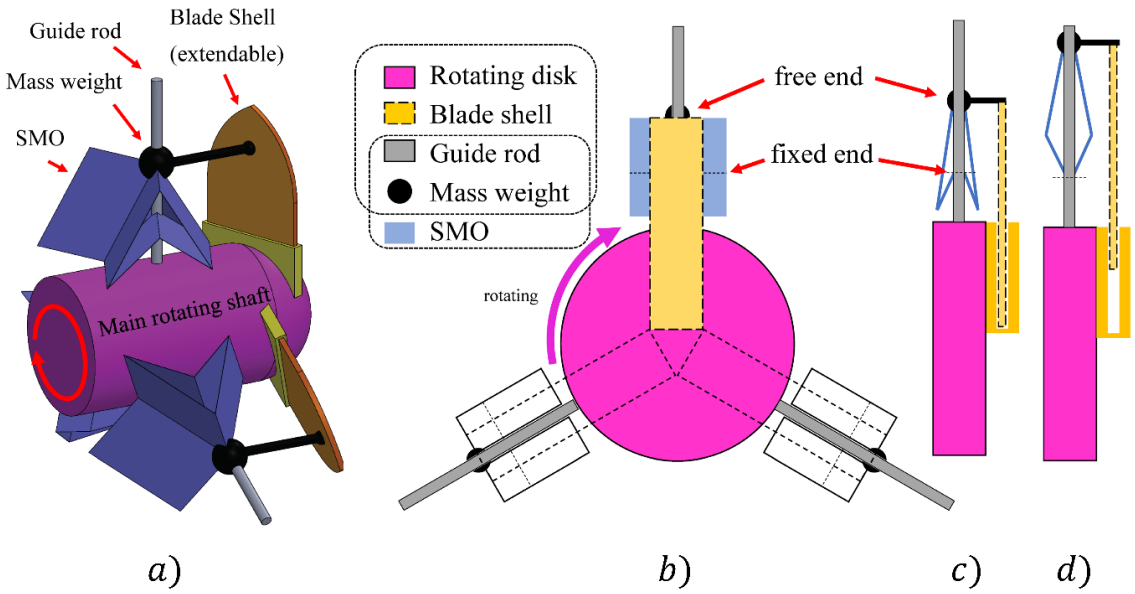

Fig. 1 Schematic design of the proposed propeller system at (a-b) the initial state with shorter length of the blade; and (c-d) side-view of the SMO structure and blades at the initial state and the expanded state

The folding techniques used for origami-based mechanism have been widely discussed under different patterns for some applications [20-24]. This paper uses the edge module trimming method and the groove compliant joints, as shown in Fig.2, to avoid the potential collisions at the creases due to their thickness and at the joint sections with the rod. Hollowing facets are adopted to minimize the undesired energy dissipation due to the air friction forces at the SMO facets and also to avoid possible deflection of the facets. The groove compliant joints can be applied to all crease sections (as shown in Fig.

2(e)) and trimming at the joint corners of each facet (the round corners in Fig. 2(d)) is used to avoid the collisions during the folding process. Membrane joints between the origami facet sheets and the slidable tubes on the guild rod are of different modes according to their folding conditions and are highlighted in red in Fig. 2(b) and (c). The facets from traditional origami structures are hollowed out to minimize the energy dissipation and aerodynamic effect during the rotation of the proposed system. Edge strength methods or directly attaching hard materials to the facet frame, as shown in Fig. 2(d), can be applied to increase the bending stiffness of the hollowed facets to ensure their rigidity.

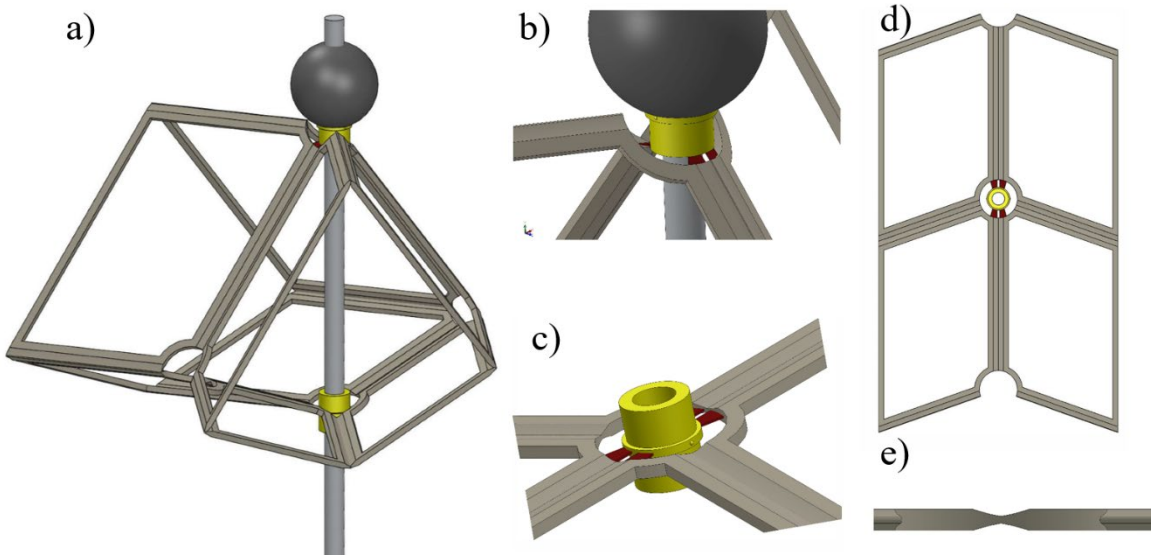

Fig. 2 Details of the SMO structure with facet trimming: (a) 3D SMO structure with mass weight; (b-d) joint sections between the SMO structure and the rod; (d) top view of the facets with edge module trimming, and (e) side view of the crease trimming

2.1 Model of the SMO structure

Since the mechanical property of the origami structure strongly relies on its geometric characteristics, the design parameters of SMO structure will be first considered. A typical SMO structure is composed of two layers of different Miura-ori cells,

as shown in Fig. 3 (a) and (b). The SMO structure has two stable states, namely convex state and concave state, as shown in Fig. 3 (c). The geometric feature of each single Miura-ori cell includes two sides of its standard facet and the sector angle. One side of the facet from each sheet at the connected facets shares the same parameter ($b_I = b_{II} = b$), and at least one of the other two parameters ((a_I, a_{II}) & (γ_I, γ_{II})) is independent. By assuming rigid origami folding condition, all facets are rigid during folding and both facet sheets are kinematically compatible. Thus, the independent design parameters should satisfy the following relationships to ensure their compatibility:

$$\frac{\cos\gamma_{II}}{\cos\gamma_I} = \frac{a_I}{a_{II}} \tag{1}$$

$$\frac{\cos\theta_{II}}{\cos\theta_I} = \frac{\tan\gamma_I}{\tan\gamma_{II}} \tag{2}$$

where θ_I and θ_{II} are the dihedral folding angles of the facets on each sheet to the reference panel (indicated by *ref panel*, as shown in Fig. 3 (b)). For clarity, the stable state is referred to as “concave” state when Sheet I is nested-in and the dihedral folding angle is $\theta_I > 0°$; and similarly, as “convex” state otherwise. There also exits a meta-stable state when Sheet I is flatted and $\theta_I = 0°$, at which the dihedral folding angle of Sheet II is minimized.

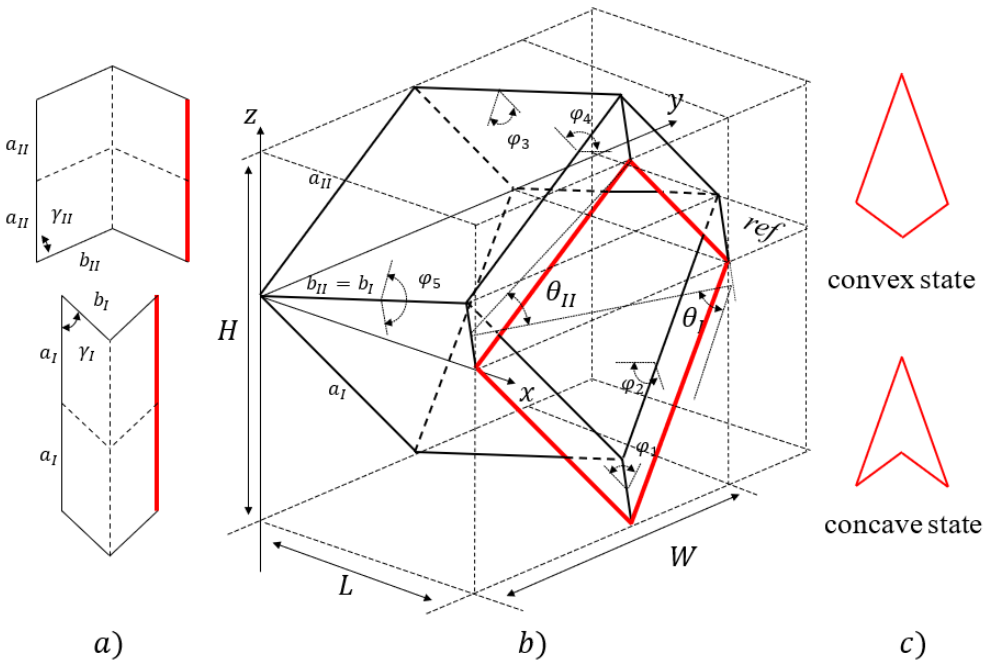

Fig. 3 Typical SMO structure: (a) Miura-ori sheets with different parameters; (b) 3D SMO structure and (c) its bi-stable states

The external dimensions of the SMO structure can be expressed by using the dihedral folding angle of the facet on Sheet I to the reference panel (θ_I), which can also be used to indicate the folding conditions [16]:

$$\begin{cases} L = \frac{2b_I \cos\theta_I \tan\gamma_I}{1+\cos^2\theta_I \tan^2\gamma_I} \\ W = 2a_I\sqrt{1-\sin^2\theta_I \sin^2\gamma_I} \\ H = a_I \sin\gamma_I \left(\sqrt{\frac{\tan^2\gamma_{II}}{\tan^2\gamma_I} - \cos^2\theta_I} - \sin\theta_I\right) \end{cases} \tag{3}$$

where L, W and H represent the length, width and height of the cell in the x-y-z directions as shown in Fig. 3(b).

The changes in each external dimension with respect to the folding condition can be calculated, as illustrated in Fig. 4. It is easy to notice that the *H* direction has the largest deformation with a wider boundary region and its deformation is unidirectional along the

folding process; while the other two directions have a symmetric deformation path to the meta-stable state when folding angle is $\theta_I = 0°$.

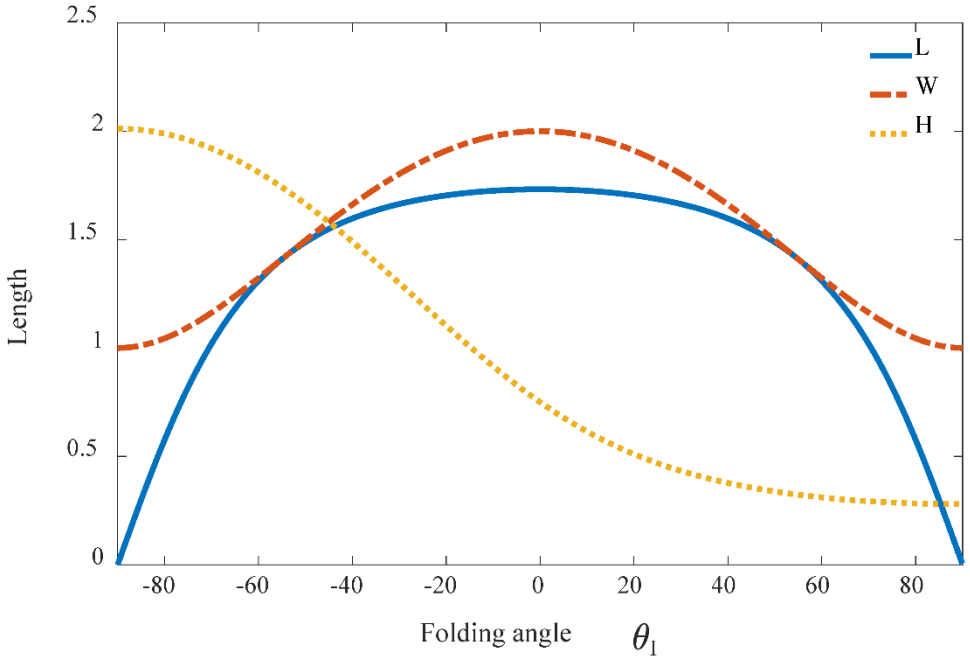

Fig. 4 The changes in the external dimensions of the SMO structure with respect to the folding condition

It is assumed that the material properties of both Miura-ori sheets are uniform but different from each other, two torsional spring stiffness per unit length (k_I & k_{II}) can be assigned to two sheets accordingly and the sharing creases at the *ref panel* are assigned with another torsional spring stiffness per unit length (k_c). Thus, the torsional spring stiffness of each crease (K_i) corresponding to its length ($l_i = a_I, a_{II}, b$) can be defined as

$$K_i = k_n \times l_i \text{ for } n = I, II, \text{and } i = 1,2, \dots ,5 \quad (4)$$

According to the folding conditions of each crease within the SMO structure, five groups of the folding angles as defined in Fig. 3 (b), can be expressed as:

$$\varphi_1 = \pi - 2\theta_I \quad (5)$$

$$\varphi_2 = 2\sin^{-1}\left(\frac{\cos\theta_I}{\sqrt{1-\sin^2\theta_I\sin^2\gamma_I}}\right) \quad (6)$$

$$\varphi_3 = \pi - 2\cos^{-1}\left(\cos\theta_I\frac{\tan\gamma_I}{\tan\gamma_{II}}\right) \quad (7)$$

$$\varphi_4 = 2\sin^{-1}\left(\frac{\sin\gamma_I}{\sin\gamma_{II}}\sin\frac{\varphi_2}{2}\right) \quad (8)$$

$$\varphi_5 = \cos^{-1}\left(\cos\theta_I\frac{\tan\gamma_I}{\tan\gamma_{II}}\right) - \theta_I \quad (9)$$

These folding angles at the creases and the geometric parameters of different sheets will be used to calculate the potential and kinematic energy of the origami structure. The total elastic energy from the bending deformations of both creases and facets is given by:

$$U_{\text{total}} = U_{\text{crease}} + U_{\text{facet}} \quad (10)$$

For the rigid origami structure, only the potential energy of the creases is considered and the bending energy of the facets is assumed to be 0. Then the total elastic potential energy of the SMO structure is the summation of each individual crease's energy, which can be calculated by the dihedral angle of each crease and the corresponding torsional stiffness K_i:

$$U_{\text{crease}} = \frac{1}{2}\sum_{i=1}^{n} K_i(\gamma_i - {\gamma_i}^0)^2 \quad (11)$$

where n is the total number of the creases within the SMO structure and ${\gamma_i}^0$ is the reference dihedral angle of the creases when the SMO structure is assumed to be under stress-free condition. The stress-free condition of the whole structure is dependent on the original pre-deformation condition of each individual crease and can be specified using the folding condition θ_I^0 (θ_0).

Fig. 5 (a) illustrates the elastic potential energy on different sheets, the sharing creases and the total energy landscape of the SMO structure according to the folding condition when the stress-free folding angle is $\theta_0 = +60°$ (at the concave state). Other design parameters are given by $a_I = b, a_{II} = 1.25b, \gamma_I = 60°,\ k_{II} = 20k_I$ and $k_c = k_I$. It is clearly shown in Fig. 5 (a) that there are two stable states (one in the concave state and the other in the convex state) and one meta-stable state (when Sheet I is flattened at meta-stable state) according to the total energy landscape. The folding angles at the two stable states can be found to have the same magnitude but opposite signs. It is also easy to observe from Fig. 5 (b) that when different stress-free folding angles are applied, the energy landscape in Sheet II is highly sensitive and the folding configuration of Sheet II is symmetric to the meta-stable condition. According to Eq. (11) and Fig. 5, increasing the crease stiffness per unit length in Sheet II (k_{II}) can have a significant impact to the bi-stable states of the SMO structure. Unless otherwise specified, the subsequent sections use the same design parameters and the stress-free folding angle $\theta_0 = +60°$ at the concave state. It is worth noting that the changes of the stress-free condition will not change the SMO geometric parameters. This means, the deformation (or shape change) according to its folding condition would still follow the same pattern even under different stress-free conditions.

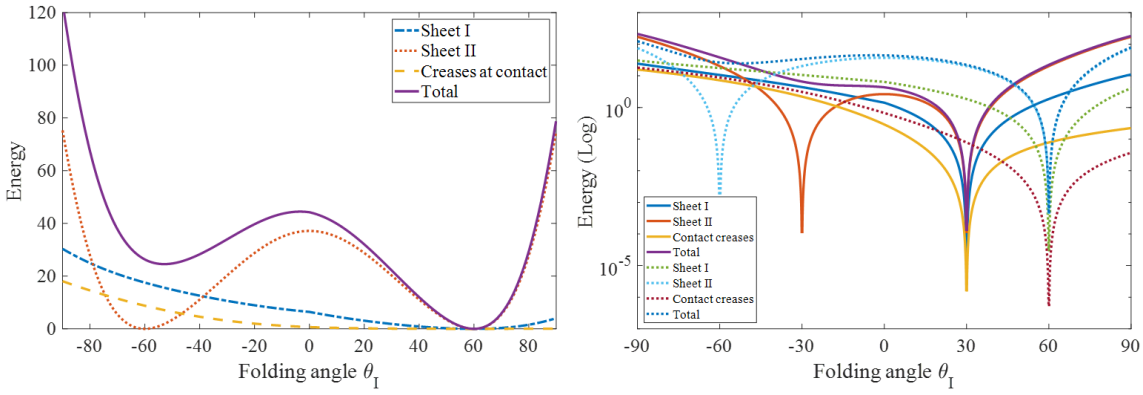

Fig. 5 Energy landscapes within the SMO structure: (a) Energy landscape for Sheet I, Sheet II, creases at contact and the overall system when $\theta_0 = +60°$, and (b) Energy landscapes when the stress-free condition is changed from $\theta_0 = 30°$ to $60°$

By differentiating the total potential energy with respect to the deformation in each principal direction (external dimension directions as shown in Fig. 3(b)), the force-deformation and force-energy relationship can be obtained as

$$F_X = \frac{dU_{crease}}{dH} = \frac{dU_{crease}}{d\theta}\left(\frac{dX}{d\theta}\right)^{-1} \quad for\ X = H, L\ or\ W \tag{12a}$$

$$U_{crease} = f_{SMO_{(F_H, F_L, F_W)}} \tag{12b}$$

According to the force-displacement relationship as shown in Fig. 6(b), snap-through behavior can be observed when negative stiffness appears in the folding process. These behaviors are similar to other bi-stable mechanisms, and a rapid self-deformation would be generated due to the elastic instability. Also because of the nonlinear asymmetric geometric correlations, the onsets of the snap-through behavior would be different during the extension and compression process. It should be noted that the snap-through behaviors do not happen immediately when the system enters into different energy branches. The bi-stable states and the snap-through behaviors are critical for

designing the morphing propeller system and they will be further discussed in the following sections.

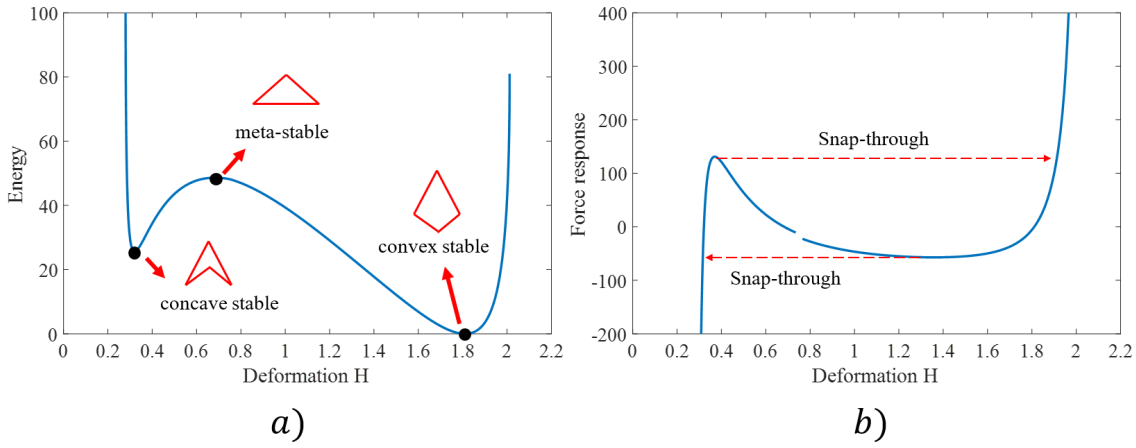

Fig. 6 (a) Energy-deformation and (b) force-deformation in the H direction of the SMO structure

2.2 Performance evaluation and comparison

It is known that for the standard propeller system, the system output, the open-water propeller thrust (*T*) and the power used for torque requirement (P) can be calculated using:

$$T = K_T \rho \omega^2 D^4, \; P = C_p \rho \omega^3 D^5 \tag{13}$$

where K_T is the thrust coefficient; ρ is the fluid density (normally in air or water); ω is the propeller rotating speed (in rev/s); D is the propeller diameter and C_p is the power coefficient.

For a given standard system, the relationships between the effective propeller diameter, rotational speed, thrust output and power usage are shown in Fig. 7. High thrust output can be achieved by increasing the rotating speed or using larger propeller

diameter (longer blades). However, the power usage would be increased with an increase of thrust output.

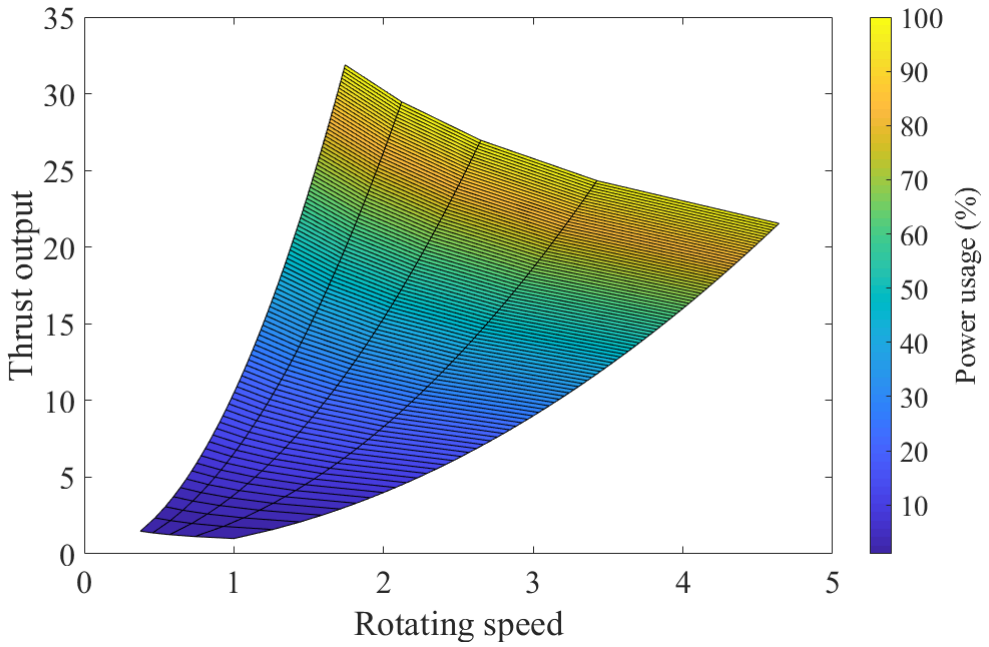

Fig. 7 Thrust output and power required for the standard propeller system with fixed length blades

When implementing the SMO structure into the propeller system proposed, a designed weight with mass m is added on the top of the SMO structure for an equivalent force distribution on the structure. The centrifugal force due to the rotation of the weight is applied to the SMO structure as an external excitation force to switch it between its two stable states. The centrifugal force (F_c) can be calculated using the initial eccentricity of the weight (d_0) and the deformation of the SMO in the height direction (dH) as:

$$F_c = m\omega^2(d_0 + dH) \tag{14}$$

where ω is the rotating speed of the system and the initial eccentricity should be larger than 0 $(d_0 > 0)$.

Considering the aerodynamic effects of the SMO-based morphing propeller structure, the deformation-rotation relationship of the proposed system, can be obtained from Eqs. (12) and (14), and is shown in Fig. 8, where the snap-through behaviors are also indicated:

$$m\omega^2(d_0 + dH) = \frac{d(U_{crease} - f_{SMO}^{-1}(f_{aH}, f_{aW}, f_{aL}))}{dH} \quad (15)$$

where f_{aH}, f_{aW}, f_{aL} are the air friction force applied on the SMO facets during rotation. When a large area is hollowed on the facets, the effective area of the facets is minimized. Thus, the air friction forces are insignificant and can be neglected in comparing with the centrifugal force (F_c). Accordingly, the wasted energy due to these air friction forces can also be ignored. It is worth noting that the extension of the blade shell is synchronized to the deformation of the SMO structure. Thus, the deformation of the system indicates the increase of the length of the blade shell and hence the effective propeller diameter is increased to ($D = 2(d_0 + dH)$).

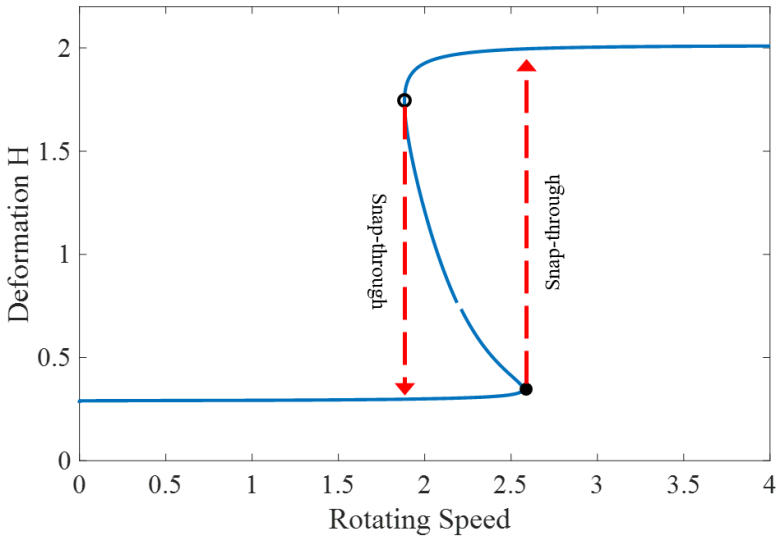

Fig. 8 Deformation-rotation relationship of the proposed morphing system

According to Eq. (13), the thrust output and power required for the proposed morphing propeller system can be calculated and illustrated in Fig. 9. The performances of two standard propeller systems with fixed length blades are also simulated and shown in the figure for comparison. The lengths of the fixed blades in two standard systems are same as the length of the morphing structure either at the initial state or at the maximum extension state. The snap-through behaviors could generate two critical points as illustrated in Fig. 9, which will be referred to here as the expansion point and the shrinkage point. When the rotating system starts from rest and the rotating speed is lower than the value at the expansion point, the system can be operated in a Low-Speed operation mode. Once the rotating speed is higher than the value at the expansion point, the system will turn into High-Speed operation mode. After entering the High-Speed operation mode, even when the rotating speed is decreasing and lower than the value at expansion point, the system will remain in High-Speed operation mode, where the SMO structure is in the convex state and the effective propeller diameter is larger. Only when the rotating speed is lower than the shrinkage point, the SMO structure will be folded to the concave state, thus the system will transform into the Low-Speed operation mode and the effective propeller diameter is smaller.

The advantage of using the proposed morphing structure can be seen from the differences between the designed performance (solid line) and the standard performance (dashed or dot lines), as shown in Fig. 9. Compared to the standard fixed propeller system, Low-Speed operation mode would have similar performance of the thrust output to the standard system with fixed initial-length blades. Slight differences of the performance are

mainly caused by the small enlargement of the SMO structure in the concave state. When in High-Speed operation mode, the thrust output of the proposed morphing structure can reach the same performance as the standard system with the fixed blades of larger length. This means that the thrust output of the proposed system at High-Speed operation mode is larger than the standard system with initial-length blades when the rotating speed of the system is between the expansion point and shrinkage point. Fig. 9(b) illustrates the power required for driving the propeller system at different rotating speeds. The area under each curve from one single rotating speed to another speed represents the energy required during the process. For example, one propeller is assumed to operate at the speed of 2.5, as shown in Fig. 9(b); the total area of Shadow 1 represents the energy dissipation when the standard propeller system (with the larger-length blades) starts from rest to the rotating speed at the expansion point. Meanwhile, due to the snap-through behavior, the area of Shadow 2 indicates the energy dissipation when the proposed propeller system starts from rest to the same rotating speed. The difference between the two shadow areas is the energy saving of the proposed system with reference to the standard blade with fixed length, which can also be regarded as the energy saving in one transition cycle. Also, the longer time stays in the Low-Speed operation mode, the more energy can be saved when transforming to the High-Speed operation mode compared to the standard propeller system.

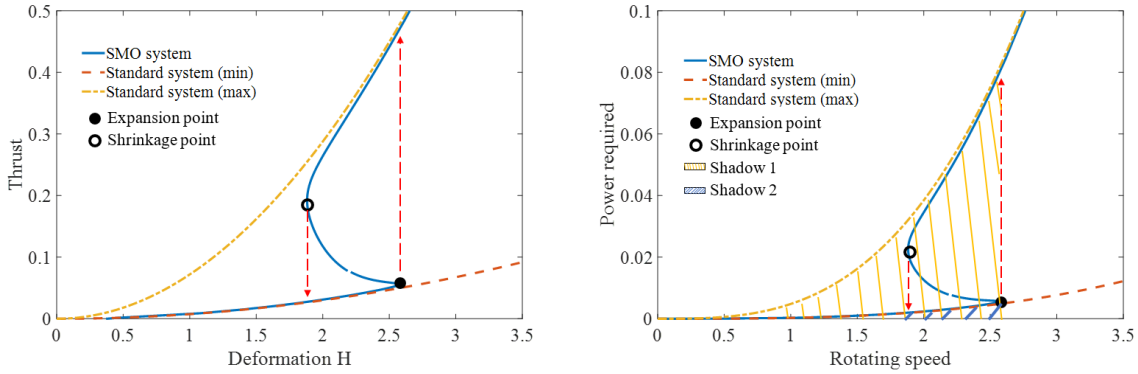

a) *b)*

Fig. 9 (a) Thrust output and (b) energy required for driving the proposed morphing propeller system compared with the standard systems

3 Effects of design parameters

In this section, the design parameters will be studied for their effects on the system performance in both thrust output and energy usage. Some design parameters are related to the SMO structure given in the non-dimensional setting, such as the independent facet sides (a_I, a_{II}), the sector angle γ_I, the stress-free condition θ^0, and the crease stiffness per unit length (k_{II}, k_c). Other parameters are independent to the SMO structure, such as the designed mass m and the initial eccentricity d_0. Meanwhile, the designing critical points of the proposed morphing propeller system are the levels of the thrust output and the power required, expansion point and shrinkage point. The levels of the thrust output and the power required are related to the length of the blades and the rotating speed. The expansion point and shrinkage point are mainly determined by the geometric parameters of the SMO structure and the force applied on it. Fig. 10(a) shows the effects of the sector angle of Sheet I (γ_I) on the deformation of the SMO structure. Both the maximum deformation and the deformable range of the SMO structure can be reduced when the sector angle γ_I is smaller. As a result, the maximum

level of the thrust output of the system will be reduced accordingly, as shown in Fig. 10(b). However, the thrust output level of the proposed system in Low-Speed mode does not change substantially. This indicates that a small sector angle γ_I could reduce the thrust output level in High-Speed mode and the energy can be saved when transforming from the Low-Speed mode to the High-Speed mode. Other design parameters that can affect the maximum deformation of the SMO structure are the side length of each sheet (a_I, a_{II}), as shown in Fig. 11. The enlargement of the facet side from either sheet $(a_I \text{ or } a_{II})$ would induce an increase at the maximum level of the thrust output. However, the effects on the thrust output at the Low-Speed mode are opposite. The enlargement of the side from Sheet I (a_I) could reduce the level of the thrust output at the Low-Speed mode and hence increase the difference between Low-Speed and High-Speed modes. On the contrary, the enlargement of the side from Sheet II (a_{II}) could increase the thrust output level at both modes at the same time.

It is interesting to note that the effects of these parameters on the critical points are similar. A smaller sector angle γ_I could reduce the shrinkage point to a lower value but slightly change the expansion point. The expansion of the side of either sheet $(a_I \text{ or } a_{II})$ could move the shrinkage point to a lower value but leads to an opposite change to the expansion point.

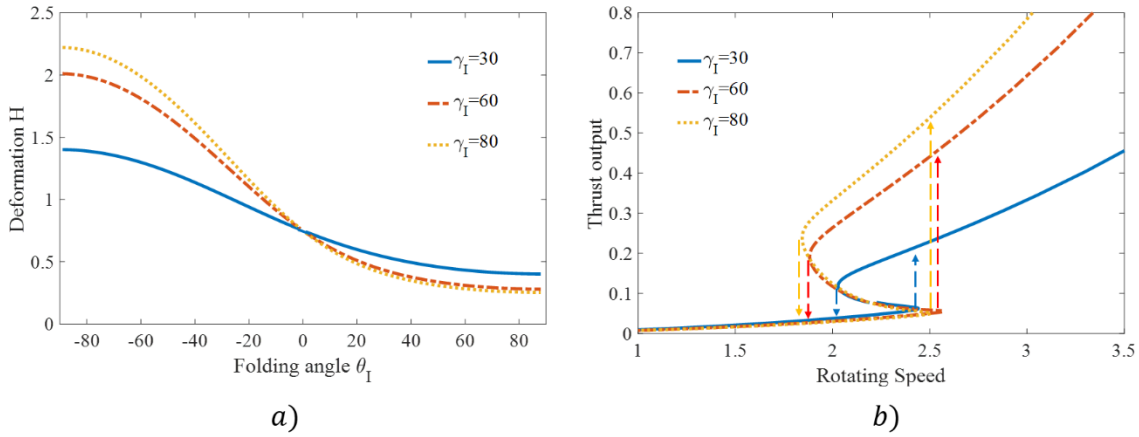

Fig. 10 Effects of the sector angle of Sheet I (γ_I) on: (a) the deformation of the SMO structure, and (b) the system performance

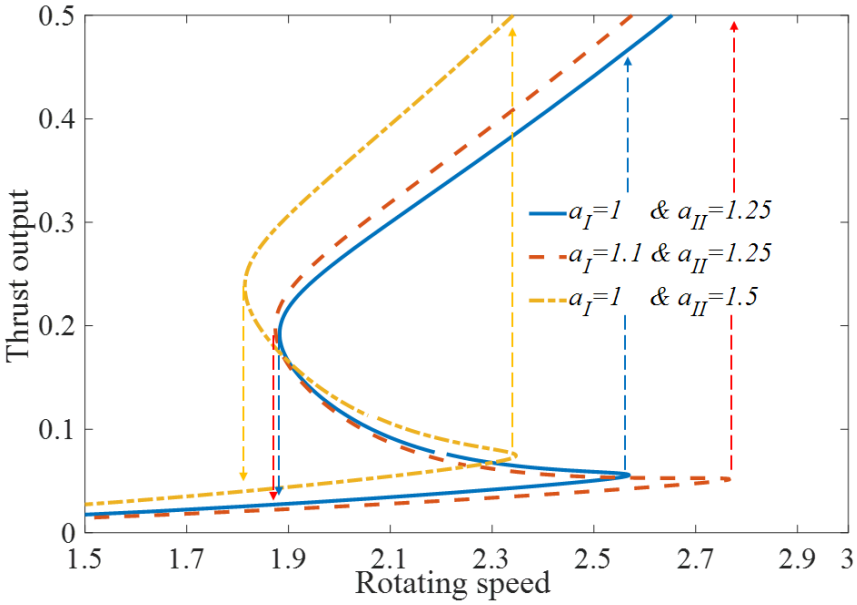

Fig. 11 Effects of independent facet side length of sheet (a_I, a_{II}) on the system performance

The stress-free condition θ_0 and the effective unit-length crease stiffness (k_i) would barely affect the geometric performances of the SMO structure, such as deformable range, but are highly related to the elastic potential energy. Thus the thrust output levels of the system at either Low-Speed mode or High-Speed mode remain unchanged but the critical points could be controlled due to the energy landscape. As

demonstrated in Fig. 5, the energy difference between the concave and convex states is larger when the initial folding condition of Sheet I is higher ($\theta_I \to \pm 90°$), and the energy landscape within the SMO structure is highly sensitive to the stress-free condition θ_0. Hence, the critical points could be controlled accordingly as shown in Fig. 12. The higher value of the stress-free condition θ_0 could increase the distance between the expansion point and shrinkage point, which increases the value of expansion point and reduce the value of shrinkage point as shown in Fig. 12(a). The energy landscape, as shown in Fig. 5, illustrates the importance of the elastic potential energy involved in Sheet I, Sheet II or the sharing creases. The changes of the effective unit-length crease stiffness (k_i) can alter the total energy landscape and hence the locations of the critical points. Fig. 12(b) shows the two ways to control these critical points: either decreasing k_{II} to lower the expansion point; or increasing k_c to rise the shrinkage point. It is worth emphasizing that the effects of either k_{II} to shrinkage point or k_c to expansion point are insignificant.

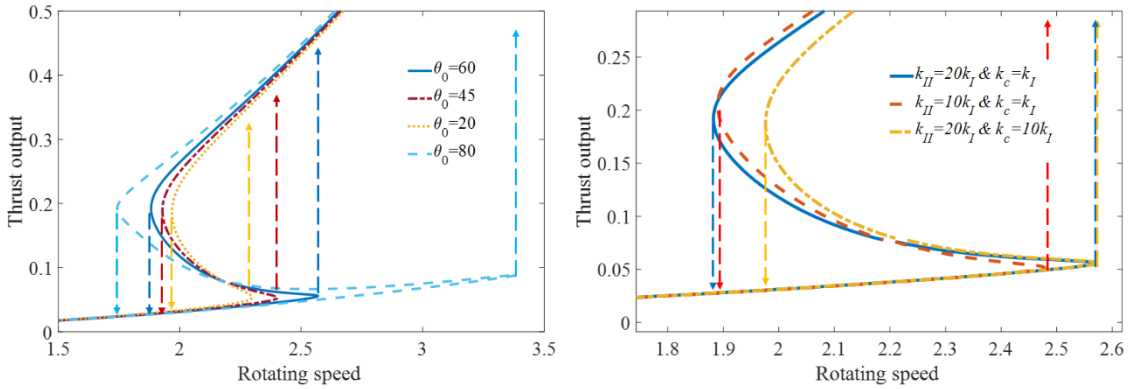

Fig. 12 Effects of stress-free condition and effective unit-length crease stiffness on the critical points: (a) Stress-free condition θ_0, (b) the effective unit-length crease stiffness k_i

There are another two design parameters apart from the SMO structure that can affect the system performance: the designed weight m and the initial eccentricity d_0. It is

easy to gain physical insights that the heavier weight and larger initial eccentricity could result in a higher centrifugal force, and then a larger shape deformation of the SMO structure. Although both parameters would not change the geometric parameters of the SMO structure, the initial eccentricity d_0 can be used to set the initial conditions of the proposed structure, where the initial-length of the blade is different. Fig. 13 demonstrates the effects of these two parameters on the system performance. The heavier weight could result in lower values of both expansion point and shrinkage point, while shorter initial eccentricity d_0 could degrade the overall performance of the system.

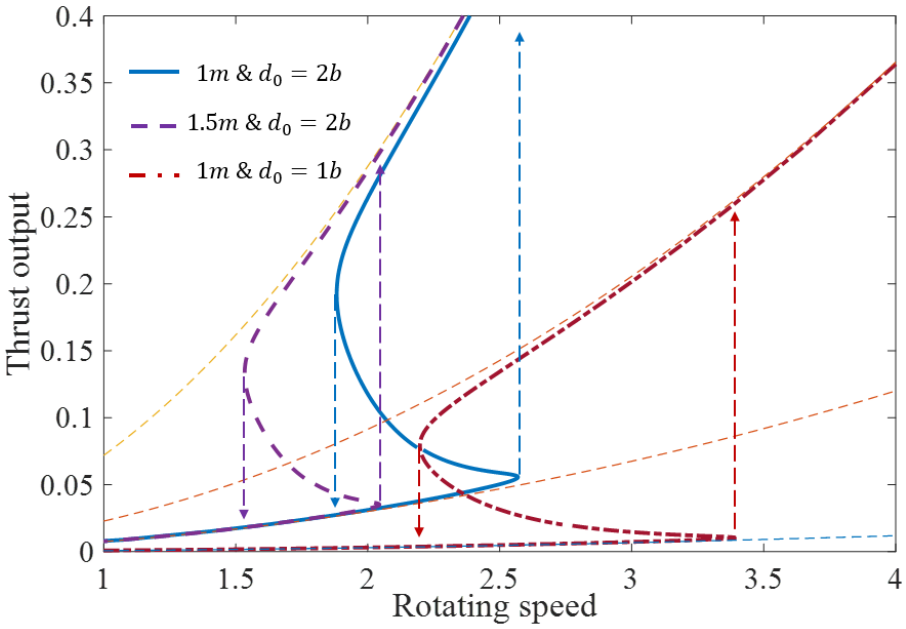

Fig. 13 Effects of the designed weight (or mass m) and the initial eccentricity d_0 on the system performance

It can be summarized that the design parameters that can affect the shape and deformable range of the SMO structure, such as facet size or their sector angle, could have a significant effect on the system performance. While the other parameters such as initial folding condition and crease stiffness that are associated with the boundary

conditions of the deformation would have less effect. Meanwhile the other system parameters irrelevant to the SMO structure are also important for the energy saving purpose, such as the designed weight and initial eccentricity.

4 Conclusion

In this article, a novel propeller system has been designed by using stacked Miura-ori (SMO) origami structure. Different from the standard propeller system with fixed length blades, origami-based structure, as a special form of morphing structure, has been developed for a rotating system to create a morphing blade system. The length of the blades could be changed to two different stages according to the rotational speed of the system. Thus, the thrust output could be improved and the energy usage saved through switching into different operation states. Edge trimming method and hollowed facets were applied on the origami structure to avoid the physical collisions and minimize the undesired energy dissipation due to the aerodynamics and air friction forces during rotating operation.

To uncover the underlying physical principles of the folding process, the geometric parameter analysis was first carried out. The energy landscapes for the components of the SMO structure were numerically simulated and compared. The bi-stabile state and the snap-through behavior during the folding process were studied to determine two critical points. The operating mechanism was then utilized in a rotating system to provide a morphing structure to change the blade's effective length. According to the effective propeller diameter and the system output (thrust output), two operating modes were defined as the Low-Speed operation mode and High-Speed operation mode. The

propeller system at the Low-Speed operation mode has a similar output level as a standard system with fixed blades, where the fixed blade length is equal to the initial-length of the blade of the proposed system at rest. At the High-Speed mode, the propeller system could produce a similar output level as a standard system with fixed blades at the maximum expanded length. Two critical rotating speed points due to its snap-through behavior were then referred to as the expansion point and shrinkage point. The expansion point was associated with the point where the rotating speed was increased from the Low-Speed mode to High-Speed mode, and the shrinkage point was related to the rotating speed which is decreased from the High-Speed mode to Low-Speed mode. In addition of the improvement on the system output level, another advantage of using the proposed morphing structure lies in its energy saving. Energy could be saved during the process when the rotating speed was passing through the critical expansion speed. The critical points could be carefully designed for some special requirements in read-world applications.

It is hoped that the results of this study would open a new avenue towards applying the origami structure in rotating systems with a similar demand, such as a fan system or wind turbine blades. Future work based on this research will be towards fabricating the proof-of-concept prototype and experimental investigation into its performance for a real-world application.

REFERENCES

[1] Barbarino, S., Bilgen, O., Ajaj, R. M., Friswell, M. I., and Inman, D. J., 2011, “A Review of Morphing Aircraft,” Journal of Intelligent Material Systems and Structures, 22(9), pp. 823-877. https://doi.org/10.1177/1045389x11414084.

[2] Lachenal, X., Daynes, S., and Weaver, P. M., 2013, "Review of morphing concepts and materials for wind turbine blade applications," Wind Energy, 16(2), pp. 283-307. https://doi.org/10.1002/we.531.

[3] Baghdadi, M., Elkoush, S., Akle, B., and Elkhoury, M., 2020, "Dynamic shape optimization of a vertical-axis wind turbine via blade morphing technique," Renewable Energy, 154, pp. 239-251.

[4] Chen, F., Liu, L., Lan, X., Li, Q., Leng, J., and Liu, Y., 2017, "The study on the morphing composite propeller for marine vehicle. Part I: Design and numerical analysis," Composite structures, 168, pp. 746-757.

[5] Blondeau, J., Richeson, J., and Pines, D., 2003, "Design of a morphing aspect ratio wing using an inflatable telescoping spar," Proc. 44th AIAA/ASME/ASCE/AHS/ASC Structures, Structural Dynamics, and Materials Conference, p. 1718.

[6] Van Dam, C., Berg, D. E., and Johnson, S. J., 2008, "Active load control techniques for wind turbines," Sandia National Laboratories.

[7] Peraza-Hernandez, E. A., Hartl, D. J., Malak Jr, R. J., and Lagoudas, D. C., 2014, "Origami-inspired active structures: a synthesis and review," Smart Materials and Structures, 23(9). https://doi.org/10.1088/0964-1726/23/9/094001.

[8] Willis, A. M., 2012, "Collapsible kayak," Google Patents.

[9] Butler, J., Bowen, L., Wilcox, E., Shrager, A., Frecker, M. I., von Lockette, P., Simpson, T. W., Lang, R. J., Howell, L. L., and Magleby, S. P., 2018, "A Model for Multi-Input Mechanical Advantage in Origami-Based Mechanisms," J Mech Rob, 10(6), p. 061007. https://doi.org/10.1115/1.4041199.

[10] Taylor, A. J., Chen, Y., Fok, M., Berman, A., Nilsson, K., and Ho Tse, Z. T., 2017, "Cardiovascular Catheter With an Expandable Origami Structure," J Med Devices, 11(3). https://doi.org/10.1115/1.4036581.

[11] Banerjee, H., Li, T. K., Ponraj, G., Kirthika, S. K., Lim, C. M., and Ren, H., 2020, "Origami-Layer-Jamming Deployable Surgical Retractor With Variable Stiffness and Tactile Sensing," J Mech Rob, 12(3), p. 031010. https://doi.org/10.1115/1.4045424.

[12] Brandon Sargent, Jared Butler, Kendall Seymour, David Bailey, Brian Jensen, Spencer Magleby, and Howell, L., 2020, "An Origami-Based Medical Support System to Mitigate Flexible Shaft Buckling," J Mech Rob, 12(4), p. 041005. https://doi.org/10.1115/1.4045846.

[13] Sung, C., and Rus, D., 2015, "Foldable Joints for Foldable Robots," J Mech Rob, 7(2). https://doi.org/10.1115/1.4029490.

[14] Banerjee, H., Pusalkar, N., and Ren, H., 2018, "Single-Motor Controlled Tendon-Driven Peristaltic Soft Origami Robot," J Mech Rob, 10(6), p. 064501. https://doi.org/10.1115/1.4041200.

[15] Firouzeh, A., and Jamie Paik., 2015, "Robogami: a Fully Integrated Low-Profile Robotic Origami," J Mech Rob, 7(2), p. 021009. https://doi.org/10.1115/1.4029491.

[16] Ji, J. C., Luo, Q., and Ye, K., 2021, "Vibration control based metamaterials and origami structures: A state-of-the-art review," Mechanical Systems and Signal Processing, 161, p. 107945. 10.1016/j.ymssp.2021.107945.

[17] Schenk, M., and Guest, S. D., 2013, "Geometry of Miura-folded metamaterials," Proceedings of the National Academy of Sciences, 110(9), pp. 3276-3281. https://doi.org/10.1073/pnas.1217998110.

[18] Fang, H., Li, S., Ji, H., and Wang, K. W., 2017, "Dynamics of a bistable Miura-origami structure," Physical Review E, 95(5-1), p. 052211. https://doi.org/10.1103/PhysRevE.95.052211.

[19] Fang, H., Wang, K. W., and Li, S., 2017, "Asymmetric energy barrier and mechanical diode effect from folding multi-stable stacked-origami," Extreme Mechanics Letters, 17, pp. 7-15. https://doi.org/10.1016/j.eml.2017.09.008.

[20] Butler, J., Pehrson, N., and Magleby, S., 2020, "Folding of Thick Origami Through Regionally Sandwiched Compliant Sheets," J Mech Rob, 12(1). https://doi.org/10.1115/1.4045248.

[21] Guo, Z., Tachi, T., and Yu, H., 2022, "Folding Process Planning of Rigid Origami Using the Explicit Expression and Rapidly Exploring Random Tree Method," J Mech Rob, 14(1). https://doi.org/10.1115/1.4051439.

[22] Kalafat, M. A., Sevinç, H., Samankan, S., Altınkaynak, A., and Temel, Z., 2021, "A Novel Origami-Inspired Delta Mechanism With Flat Parallelogram Joints," J Mech Rob, 13(2). https://doi.org/10.1115/1.4048917.

[23] Seymour, K., Bilancia, P., Magleby, S., and Howell, L., 2021, "Hinges and Curved Lamina Emergent Torsional Joints in Cylindrical Developable Mechanisms," J Mech Rob, 13(3). https://doi.org/10.1115/1.4049439.

[24] Zhang, Q., Li, Y., Kueh, A. B. H., Qian, Z., and Cai, J., 2021, "Folding responses of origami-inspired structures connected by groove compliant joints," J Mech Rob, pp. 1-12. https://doi.org/10.1115/1.4052803.

Figure Captions List

Fig. 1 *Schematic design of the proposed propeller system at (a-b) the initial state with shorter length of the blade; and (c-d) side-view of the SMO structure and blades at the initial state and the expanded state*

Fig. 2 *Details of the SMO structure with facet trimming: (a) 3D SMO structure with mass weight; (b-d) joint sections between the SMO structure and the rod; (d) top view of the facets with edge module trimming, and (e) side view of the crease trimming*

Fig. 3 *Typical SMO structure: (a) Miura-ori sheets with different parameters; (b) 3D SMO structure and (c) its bi-stable states*

Fig. 4 *The changes in the external dimensions of the SMO structure with respect to the folding condition*

Fig. 5 *Energy landscapes within the SMO structure: (a) Energy landscape for Sheet I, Sheet II, creases at contact and the overall system when* $\theta_0 = +60°$*, and (b) Energy landscapes when the stress-free condition is changed from* $\theta_0 = 30°$ *to* $60°$

Fig. 6 *(a) Energy-deformation and (b) force-deformation in the H direction of the SMO structure*

Fig. 7 *Thrust output and power required for the standard propeller system with fixed length blades*

Fig. 8 *Deformation-rotation relationship of the proposed morphing system*

A point-to-point response to the reviewers' comments

First of all, we would like to thank the two reviewers for their time and valuable comments, on which the quality of the submitted manuscript can be improved. The manuscript has been revised by addressing the issues raised by the two reviewers.

For your convenience, in this response, the comments from the reviewers are in black, while our responses are in Red. All the revision from the last submission have been highlighted in the manuscript.

Reviewer #1 Comments

A novel propeller system with morphing blade structure for higher thrust output and energy efficiency in operations is presented in this paper. The proposed morphing propeller system shows the potential improvement on the system performance and energy efficiency, but it's not structurally innovative enough. Also, the description of the structure is not clear and detailed enough to adequately reflect the expected applicability.

The following suggestions are proposed for the author to improve the original manuscript:

(1) The abstract does not clearly reflect the purpose of the research. Please reorganize the abstract according to the hierarchy of "the purpose, methods, results and conclusions".

Authors' Response: We would like to express our apologies for not having made this clear in the manuscript. The Abstract, introduction, conclusion and related section have been rewritten in the revised manuscript.

(2) It's mentioned in the Introduction that the proposed novel system can be applied and replace some existing structures with specific requirements on nonlinear system output. However, the propeller coefficients per unit length associated with its thrust

output and the torque required are assumed to be constants in Section 2. Please further elaborate on the rationality of the simplification.

Authors' Response: We would like to express our apologies for the misunderstanding of the propeller coefficients. It is assumed that the propeller characteristics, such as aerofoil and tip angle, along the blade are unchanged. Thus, the propeller coefficients associated with thrust output and torque required are constants. With increasing the effective blade length, the thrust output and torque required will increase proportionally. The related texts have been revised in the revised manuscript.

(3) More details of the proposed structure need to be explained, such as the limiting and positioning structure of the blade shell in the unstable state.

Authors' Response: Thank you for pointing out this issue and we have provided more explanations. The synchronization of the blade shell and the SMO structure is designed using sliding components. For example, in Figure 1, the blade shells are freely sliding within their hub. The limiting and positioning are both depending on the height of the SMO, where the height is determined by the centrifugal force of the mass and the SMO force response. The unstable state during motion can be observed as fast snap-through phenomenon.

(4) The format of this paper is not standardized enough. Please double check the formatting issues and correct them.

Authors' Response: Thanks for pointing out this issue, and the format has been changed.

(5) The authors should pay particular attention to English grammar, spelling and sentence structure so that readers can clearly understand the goals and results of the research.

Authors' Response: Thanks for pointing out this issue. We have corrected some grammatical mistakes and spelling, and rewritten some sentences.

Reviewer #2 Comments

(1) In the second version, the authors have revised most of the comments. However, I don't think the mechanical design solves the collision problem. Referring to Fig. 1, the mass weight can slide along the guide rod. If I am right, there are four panels connected at the mass weight, and the angles between these panels are changing when the SMO structure is moving along the guide rod. In this case, the panels and the mass weight may have collision problems. Similarly, the bottom of the SMO structure also have collision situation. How to make the SMO mechanism to fold and slide freely along the guide rod without any physical collision?

Authors' Response: Thank you very much for pointing out this issue and we would like to express our apologies for not having made this clear in the manuscript. In origamis-based structure design, collision may potentially occur in the movement of the structure. Usually the edge trimming method is applied to cut the edge of the folding convex to avoid the collision of the facets. In this paper we adopt the edge trimming method to cut off the edges which may otherwise potentially collide and make a contact at the vortex position. A new figure has been added to provide a trimming method for solving the collision problem. As it can be seen from the figure, due to the removal of the materials at edges, the facets would not collide at the extreme folding position.

(2) I also worry about the air friction force. The SMO composed of several panels, that will increase air friction force and waste the energy. When the propeller is rotating with a high speed, the panels may have some bending deformation caused by the air friction force. Since these panels may be made of some elastic material. These issues make this system hard to work at the idea situation.

Authors' Response: Thanks for pointing out these issues and we are sorry for not discussing this in the manuscript. We agree with you. The aerodynamics of the SMO structure is very complicated due to its deployment: the position of each facet is changing with time during the morphing process. A rigorous analysis and calculation would be in its essence a good research topic, i.e., the aerodynamics and friction effect on moving

facet. To avoid or minimize the effect of air friction force, in this paper, we improved our design by removing the materials of facets and retaining the crease structure. A new figure and the corresponding explanation have been added in the revised paper to show a possible solution. By trimming and hollowing the facet, the air friction force can be minimized and the only friction force on the crease could be ignored due to a small area facing on the air flow direction. The related force response is given in Equations (12b) and (15) for discussion.

(3) The units of some parameters in several Figures are missing, e.g., energy in Fig. 5, Thrust output in Fig. 6, Deformation and rotating speed in Fig. 7, also in Fig. 8-12.

Authors' Response: Thank you for pointing out these issues and we are sorry for not discussing this clearly in the manuscript. Most of the results shown in the figures are normalized. This paper uses unit parameters in the design, such as unit length b, mass weight m, thrust and power coefficient Kt and Cp. The simulation results such as energy, thrust output and deformation are given in the normalized units, i.e., unidimensional. For example, the deformation is given by (H/d), and the thrust output is given by T/(Kt*ρ*d^4). The only non-normalized parameters are the folding angle and the rotating speed in rev/s.

It is hoped that the above has answered your concerns and questions. Thank you very much for your time and efforts.